World Conference on Timber Engineering Oslo 2023

EXPERIMENT ON AXIAL CAPACTY-BENDING CAPACITY RELATIONSHIP OF STEEL BAR-TIMBER COMPOSITE COLUMN

Keisuke Hayata[1], Motohiro Mukai[2], Shinich Shioya[3]

ABSTRACT: In light of the current climate crisis, there has been much recent interest in using timber structural members in large buildings, because timber is as renewable natural resource, and moreover, in severe earthquake prone, such as Japan, they are more desired on the grounds of light weight of timber members. We are developing a frame system formed by timber members reinforced by deformed steel bars, i.e., rebars using epoxy resin adhesive and have already developed a technique for the connection between column of ground floor and reinforced concrete foundation. Performance of the column was reported in the previous WCTE2021. We have planned an experiment to investigate bending characteristic of the other portion except hinge of the column bottom. This paper reports the experiment, its results, and comparison of experiment result and calculation on bending moment capacity.

KEYWORDS: Composite timber, Column, Deformed steel bar, Bending moment capacity, Yield moment

1 INTRODUCTION

S.Shioya, (author [3]), has proposed a structural system for building construction, adopting Hybrid Glulam Timber members using Steel bars (HGTSB, nicknamed "Samurai" in Japan) and has developed the structural design methodology [1]. Our team is now developing more refined and more competitive and commercial structural system for buildings adopting HGTSB and its structural design methodology.

2 BACKGROUND AND TARGET

S.Shioya has already developed a technique for rigid connection of rebars inside the composite timber, using carbon fiber plastic sleeve (CFS) and epoxy resin adhesive with works similarly to work process of the glued-in-rod, and reported performance of the column adopted the technique [1]. And then his group testified the application of the technique to the connection between column of ground floor and reinforced concrete foundation, by loading test of column specimens [1,2].

Figure 1(a)-(b) illustrate cross-section and side view of one specimen of an experiment [2], which is modelled for mid-rise buildings with a half-sized scale. Figure 1(c) and (d) show horizontal force-deformation angle relationship of a specimen and bending moment-rotation relationship of its footing's hinge. Yellow line relationship indicates one calculated for a conventional glulam timber column with no rebar, same cross-section, and rigid-fixed end. Light black line indicates experimental loops. The connection is found to produce high bending capacity and abundant-energy dissipation up to large deformation. Red line indicates skeleton curve calculated by the method mentioned in the previous literature [2]. The method has accurately estimated yielding moment and bending capacity of bending hinge of HGTSB column. On the other hand, the method for estimating those moment and capacity for the portion except the hinge in column, also is required. The aim of this study is to develop the method for estimating bending characteristic of the portion and the column of story above second story in building.

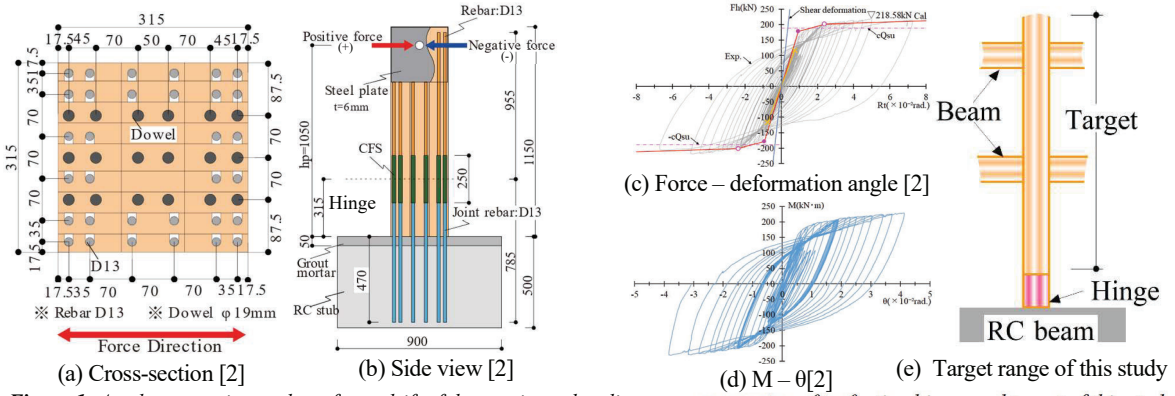

(a) Cross-section [2] (b) Side view [2] (c) Force – deformation angle [2] (d) M – θ[2] (e) Target range of this study

Figure 1: *A column specimen, shear force-drift of the specimen, bending moment-rotation of its footing hinge, and target of this study*

[1]Keisuke Hayata, Department of Architecture, Kagoshima University, Japan, k2923135@kadai.jp
[2] Motohiro Mukai, Department of Architecture, Kagoshima University, Japan
[3] Shinichi Shioya, Department of Architecture, Kagoshima University, Japan, k7347039@kadai.jp

https://doi.org/10.52202/069179-0416

3 COMPRESSION TEST

3.1 SPECIMEN

Figure 2 illustrates cross-section and side views of specimen. The scale was 1/4. Area ratio of rebars/ 8-D13 to column's gross-area/150mm x 150mm was 4.5%.
The number of specimens was to be 5 for conventional glulam timber column and 5 for the composite column. Glulam timber was prepared according to Japanese Ceder, E65-F225, in Japanese Agriculture Standard (JAS); its laminas had no joint such as finger joint. Table 1 lists mechanical properties of lamina by tests; bending strength of the lamina was 49.0N/mm^2. Rebar grade was SD345; tensile yielding strength was 384N/mm^2; ultimate tensile strength was 553N/mm^2. The adhesive for the rebar was epoxy resin adhesive with allowable upper temperature of 110℃. The process of embedding rebars adhered to the same way as Literature [3].

3.2 LOADING AND MEASUREMANT

Figure 4 illustrates set-up for loading and measurement. Monotonic compression was loaded using Amsler compression testing machine (Capacity=2MN). Axial compression force, axial deformation of overall of specimen, and axial strain of timber surface were measured.

3.3 RESULTS

Table 3 lists experimental and calculated results.

3.3.1 Failure

Figure 5 illustrates final failures; Figures 5(a)-(c) are WO specimens and Figures 5(d)-(f) are HW specimens.

i) Glued laminated timber specimen (WO)

In WO-4 in Fig. 5(b), vertical cracks appeared in wood at an axial force of 570 kN and after then the cracks developed along the wood grain. Eventually, the wood grain was crushed in middle region of specimen height, resulting in grain bending. In WO-5 in Fig. 5(c), portion of fracture was at the top, but the fracture was similar to that of WO-4.

ii) Composite timber specimen (HW)

The fracture condition of HW-3 is shown in Figure 5(e). Vertical crack occurred at axial force of 959 kN and then the crack developed along the rebar as the force increased. Portion of fracture was at the top. The fracture of HW-5 is shown in Fig. 5(f). Fracture was at the bottom. It can be seemed that location of local defects due to wood heterogeneity would be starting point of the fracture.

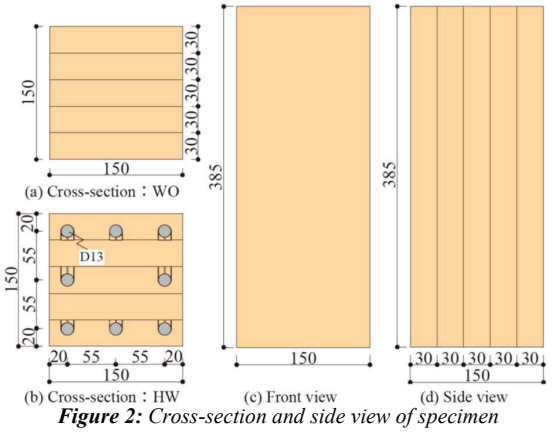

Figure 2: *Cross-section and side view of specimen*

Table 1: *Mechanical properties of lamina*

Unit: N/mm^2

Grade	Compression		Tension		Bending	
	Ec	Fc	Et	Ft	Eb	Fb
L50	5421(6)	25.2(11)	5640(5)	32.3(10)	6396(6)	49(11)

Ec,Et,Eb: Young's modulus, Fc, Ft, Fb: Strength, ( ): The number of testpeice

Table 2: Mechanical properties of rebar

Unit: N/mm^2

Diameter	a_o *in mm*^{2}	E	σ_y	σ_B
D13	126.7	1.88x10^5	384	553

a_o: Nomial cross-sctional area of rebar
E: Young's modulus, σ_y : Yielding strength
σ_B: Braking strength

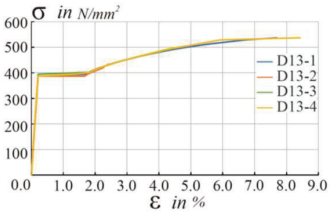

Figure 3: *Rebar in tension*

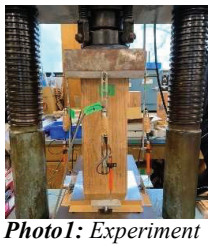

Photo1: *Experiment situation*

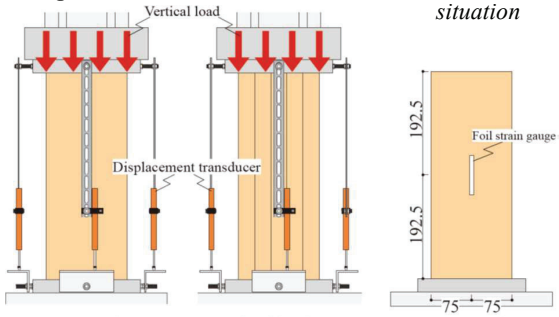

Figure 4: *Set-up for loading and measurement*

Table 3: *Specimens, experimental results, and calculation results of Compression loading test for column*

Specimen	B: Width	D: Depth	Height	The number and diameter of rebar	P_g	$_eF_m$	$_e\sigma_c$	$_cF_m$	$_c\sigma_c$	eFy	ε_p	ε_m	ε_{90}	ε_u	E	Failures
	in mm				%	*in kN*	*in N/mm*^{2}	*in kN*	*in N/mm*^{2}	*kN*	*in ×10*$^{-6}$	*in ×10*$^{-6}$	*in ×10*$^{-6}$	*in ×10*$^{-6}$	*in N/mm*^{2}	
WO-1	150.6	150.5	385.3	–	0.00	579	25.6			324	3028	10563	12661	16866	4900	
WO-2	150.7	150.5	384.6	–	0.00	579	25.6			334	2998	9047	13845	17363	5450	
WO-3	150.7	150.4	385.6	–	0.00	579	25.6	581 of average	25.6 of average	339	3352	10649	13779	15125	5200	Cruching of wood
WO-4	150.7	150.4	384.8	–	0.00	579	25.6			350	3247	10496	22164	26705	5150	
WO-5	150.7	150.2	385.3	–	0.00	586	25.9			351	3010	9126	17574	28369	5900	
HW-1	150.7	150.2	382.9	8-D13	4.48	890	39.3			654	2291	16087	16665	18462	14150	
HW-2	151.0	150.0	382.3	8-D13	4.48	952	42.1			670	2544	10711	25422	29166	13900	
HW-3	150.7	150.2	383.1	8-D13	4.48	963	42.6	944	41.7	679	2554	13062	23592	22358	14100	Cruching of wood and buckling of rebar
HW-4	150.9	150.0	381.5	8-D13	4.48	941	41.6			659	2375	8347	18422	24897	14100	
HW-5	150.6	150.3	382.8	8-D13	4.48	949	41.9			649	2435	12128	22805	23957	14100	

P_g:Aria ratio of total rebar to b-D, $_gF_m$: Axial capacity in experiment, $_e\sigma_c$: Axial stress as $_eF_m$ divided by b-D, $_cF_m$: Axial capacity caculated, $_c\sigma_c$: Axial stress as $_cF_m$ divided by b-D, $_eF_y$:Yeilding load in experient, ε_p: Strain at proportional limit, ε_m: Strain at maximum capacity, ε_{90}: Strain at reaching 90% of $_eF_m$ after maximum capacity, ε_u : Starin at finish of laoding, where these starin were calculated from data by displacement transducer.

https://doi.org/10.52202/069179-0416

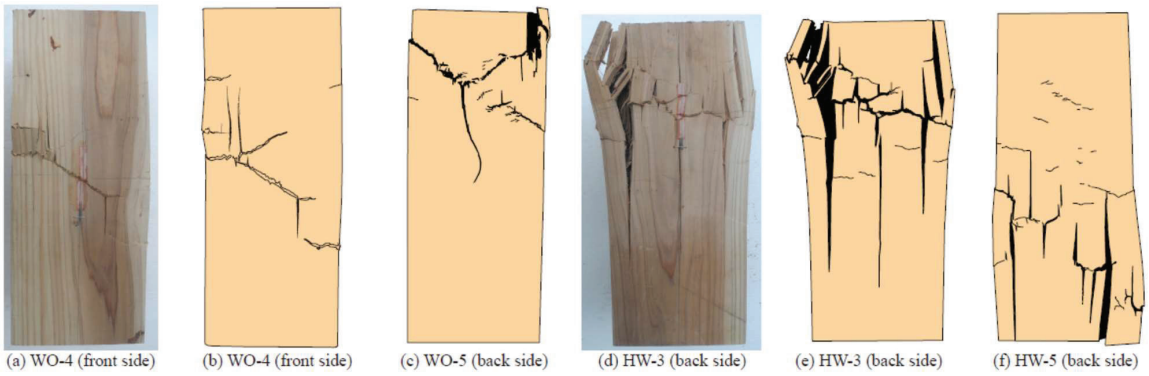

Figure 5: *Final failures*

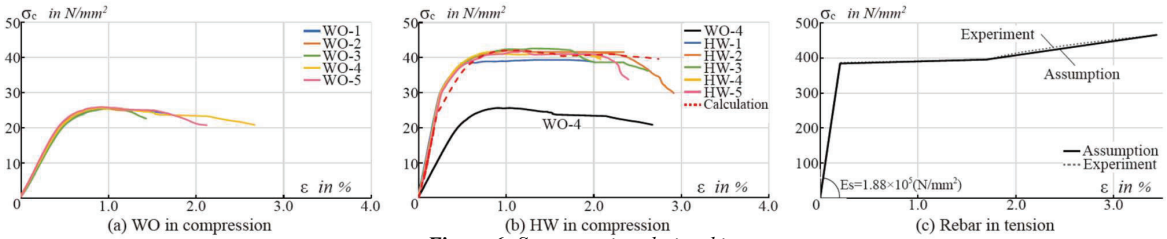

Figure 6: *Stress-strain relationships*

3.3.2 Compression stress-strain curve

The stress-strain relationship is shown in Figure 6. Vertical axis is taken as the compressive force divided by gross area of column (150x150mm), while horizontal axis is taken as the average deformation of the displacement transducers divided by height of column (385mm).

i) Glulam timber specimen (WO)

Figure 6(a) shows compressive stress-strain relationship of WO specimen is shown; those of the five specimens was similar stress-strain relationship.

ii) Composite timber specimen (HW)

Figure 6(b) shows compressive stress-strain relationships of HW specimen in comparison with that of WO-4, where the HW specimen had significantly increased elastic stiffness, compressive strength, and limit strain at which the compressive strength can be maintained (hereafter referred to as limit strain) in comparison with those of WO-4. Compressive strength increased by a factor of nearly 1.7 and was maintained up to a range of 2.0-3.0% in compressive.

3.4 ESTIMATION of COMPRESSIVE STRESS-STRAIN RELATIONSHIP

In Figure 6(b), a red dash line indicates a stress-strain relationship calculated, by assuming stress-strain curve for wood being the same as that of WO-4 and that for rebar as a curve shown in Figure 6(c) based on the results of Table 2 and Figure 3. The calculated stress-strain relationship is seen to estimate initial stiffness and compressive strength of experimental result. The point at which experimental capacity start to decrease against calculated one might be thought to be that at which buckling of rebars within column occurred. It might be thought that axial force of rebar increased as the capacity of the timber decreased, causing the rebar to buckle. The amount of decrease in the capacity of timber is thought to be a key to identifying the point at which buckling of the rebar occurs.

4 BENDING TEST

4.1 SPECIMEN

Figure 7 illustrates configuration of specimen. Scale, cross-section, and material were the same as the compression test mentioned above. Direction of bending was selected to be parallel to gluing layer of lamina, i.e.,

Table 4: *List of specimens*

Specimen	η	N *in kN*
HW(NM)-0.0	0.00	0.0
HW(NM)-0.0-B	0.00	0.0
HW(NM)-0.1-B	0.10	57.6
HW(NM)-0.2-A	0.20	115.2
HW(NM)-0.4-A	0.40	230.4
HW(NM)-1.04-B	1.04	600.0

η : Ratio of axial force N : Axial force

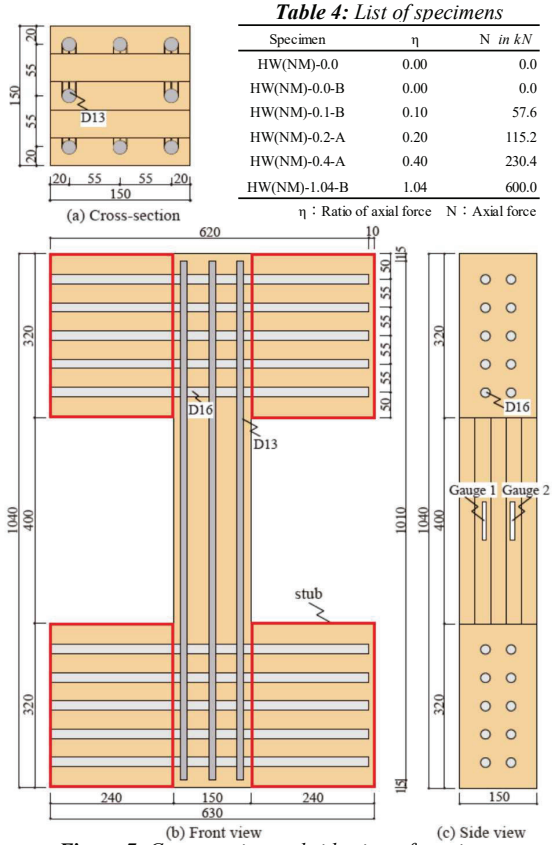

Figure 7: *Cross-section and side view of specimen*

https://doi.org/10.52202/069179-0416

weak-axis direction. Upper and lower portions of the specimen were bound to four timber stubs, with a connection using Glued-in-rod. The section between the upper and lower stubs was tested.

Table 4 lists specimen names, ratios of axial force to compressive capacity assumed, and axial forces acted. The specimen was one type of steel bar-timber composite column and the number of it was 6. Variable of specimen was magnitude of axial force, i.e., vertical force. The name of specimen was HW(NM), charged with a numerical value 'η' representing axial force ratio.

As described in later Section 4.4.1, consideration of failure of the first specimen led to adhesion of steel plate A or steel plate B to both sides of the stubs. The same adhesive as that used for the rebar was also used for these plates. Names of specimen to which the steel plates were bonded were additionally marked with the symbol 'A' or 'B' for the steel plate.

The axial force ratio was assumed to be ratio of the constant vertical load divided by average compressive capacity of the composite specimens of the compression test mentioned above. The specimens were manufactured at the same time as the specimens of the compression test.

4.2 LOADING AND MEASUREMANT

Figure 8 and Photo 2 illustrate set-up for loading of combing compression with bending. The stub was fixed with high-tension PC bar, to upper or lower H-shaped steel beam. The apparatus including a specimen was placed into other Amsler compression testing machine (Capacity=2MN) for long column. The loading was conducted to be exert a specified constant compression and to exert bending moment on it by both oil jacks up to ultimate capacity while maintaining the magnitude of the axial force. One-way pin was connected to connections between testing machine and the upper and lower H-shaped beams. Lateral braces were connected between upper stub and lower stub to prevent specimen from being out of plane. Figure 9 illustrates positions of foil strain gauges and measuring sections of deformation by displacement transducers. Foil strain gauges (measuring length: 60 mm) were adhered to surface of the wood. Two strain gauges were adhered to both surface in tensile and compressive surface; one strain gauge was adhered to side surfaces. The position of displacement transducers was changed between the upper and lower stubs in relation to

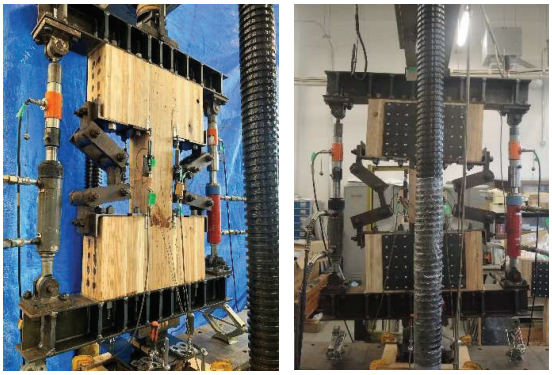

Photo2: *Set-up for loading*

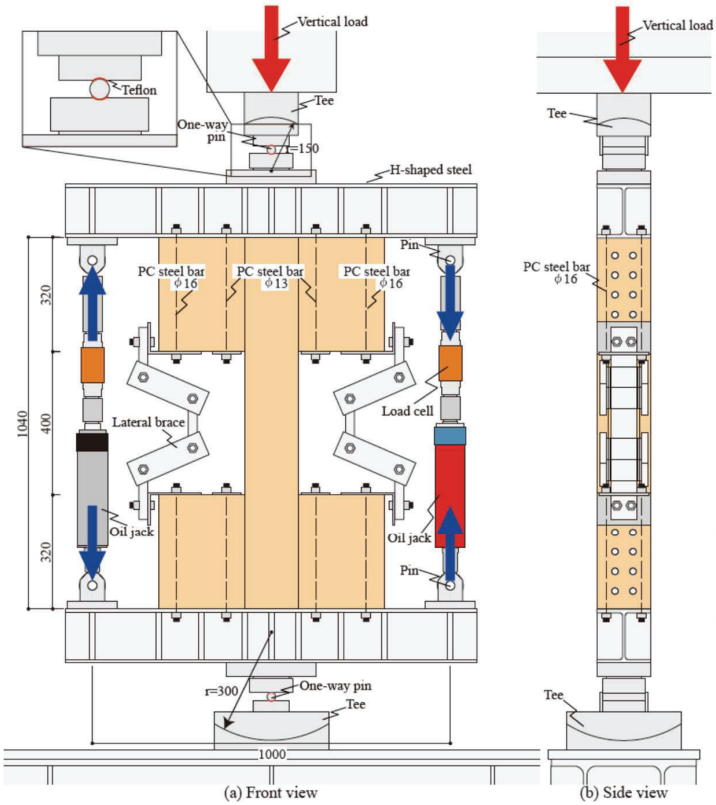

Figure 8: *set-up for loading*

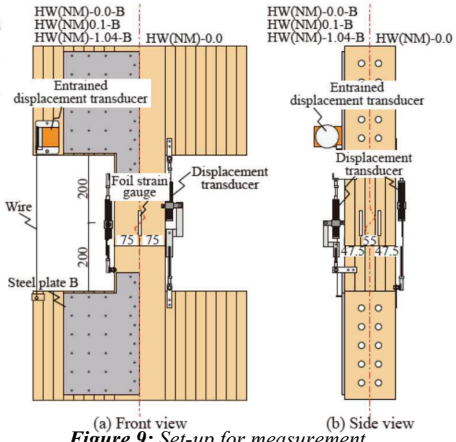

Figure 9: *Set-up for measurement*

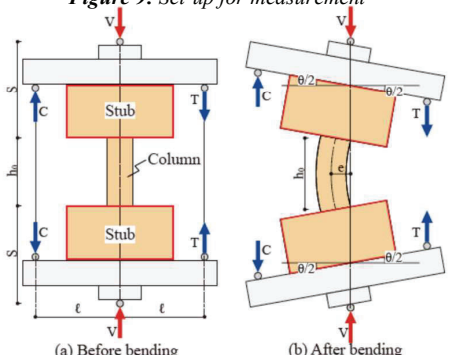

Figure 10: *Deformation of specimen under bending force*

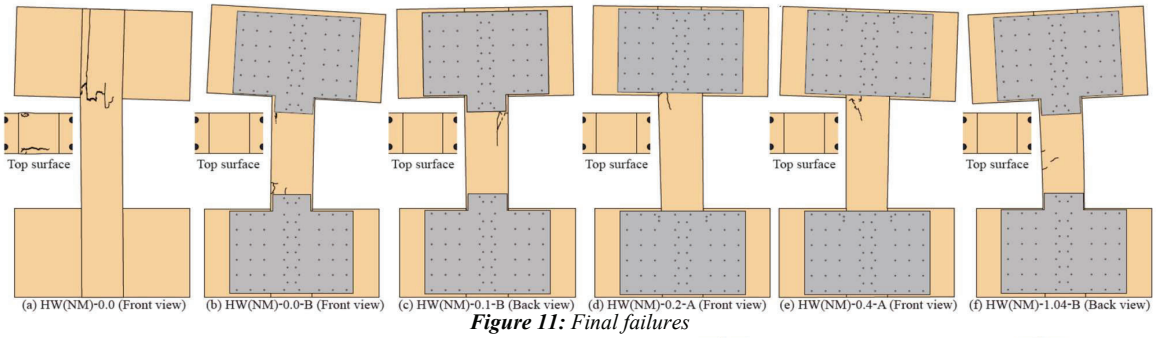

Figure 11: *Final failures*

the steel plates reinforcing the stubs. For the specimens adopting steel plate B, which will be described in Section 4.4.3, in addition to the displacement transducers, two entraining-displacement transducers were installed at both ends of the stub so that deformation due to cracks by bending could also be measured to be included.

4.3 BENDING MOMENT OF COLUMN

Figure 10 illustrates deformation of specimen under bending force. When moment is exerted on the section between the pins, cross-section at the middle height of column moves horizontally from its initial position. The horizontal distance is designated as eccentricity distance/e. An additional moment/ V・e also acts on the section due to the vertical force/V. The maximum moment/M_u is expressed as Equation (1), and the additional moment increases as the vertical force/V is increased.

$$M_u=C\cdot(\ell-e)+T\cdot(\ell+e)+V\cdot e \quad (1)$$

where C: compressive force of the oil jack for bending force, T: tensile force of the oil jack for bending force, ℓ : horizontal distance from the one-way pin to the oil jack, e: horizontal distance from line of action of the vertical load to centroid of cross-section at the middle height of the column, V: vertical force.

As the eccentricity distance/e was not measured in this experiment, it was calculated from the curvature by strain of wood or the angle of rotation between the upper and lower stubs. The curvature was taken as value by the foil strain gauge on wood and the angle of rotation was taken as value from the displacement transducer. Section/S in Figure 10(a) from center of rotation of the one-way pin to the border of column was assumed to be as rigid. Because the column is under bending and axial force, the eccentricity distance/e is expressed in Equation (2) using curvature/ϕ and in equation (3) using rotation angle/θ, on the basis of deformation of specimen.

$$e_s=S\cdot\phi\cdot h_o/2+(\phi\cdot h_o/2)\cdot(h_o/4) \quad (2)$$

$$e_d=S\cdot\theta/2+(\theta/2)\cdot(h_o/4) \quad (3)$$

4.4 RESULTS

4.4.1 Failure and strengthening of stub

Figure 11(a) illustrates failure of specimen HW(NM)-0.0 with zero axial force. This is the first specimen which was tested. Vertical cracks progressed along tensile rebars

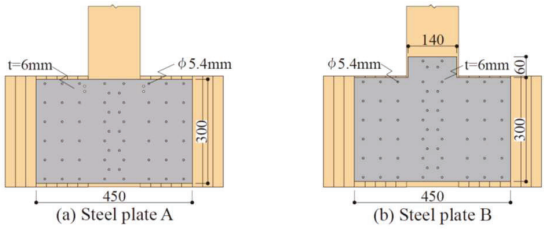

Figure 12: *Shape and dimensions of steel plate*

within the stub at near maximum load capacity; finally, anchorage failure of rebar occurred. Split cracks were observed on top surface of column after having removed the specimen from the apparatus, as shown in Figure 11(a). In buildings, the anchorage length of rebar is significantly ensured because columns are continuous in several stories. Because purpose of this study is to estimate bending capacity, steel plate A shown in Figure 12 (a) was bonded to side surface of the stubs in order to prevent the crack along rebar. It was employed for specimens with axial force ratios of 0.20 and 0.40. These specimens were named as HW(NM)-0.2-A and HW(NM)-0.4-A. Figures 11(d) and 11(e) illustrate final failures of specimens/HW (NM)-0.2-A and HW(NM)-0.4-A. The cracks along rebar occurred slightly and no cracks were observed at the top and bottom surface of column. Considering of these failures, the shape of steel plate was further modified as shown in Figure 12(b). These three specimens were HW(NM)-0.0-B, HW(NM)-0.1-B, and HW(NM)-1.04-B with axial force ratios of 0.00, 0.10 and 1.04, respectively. Figure 11(b) illustrates failure of specimen HW(NM)-0.0-B bonded with steel plate B. Cracks by bending occurred and reached maximum capacity of higher amount. Figure 11(f) illustrates failure of HW(NM)-1.04-B, in which the axial force was increased up to an axial force ratio of 1.04. No crack was observed in tensile surface, and a slight swelling was observed in wood portion in compression.

4.4.2 Moment-curvature relationship

Figure 13 shows moment-curvature relationship. The moments according to Equation (1) and (3) are shown as a solid line, and the case where the eccentricity distance 'e' is set to zero is shown as a dotted line. The assumption of e=0, after reaching the maximum bending moment, was selected on the ground of those failures which were concentrated near the borders between the stub and the column section. The moment of the solid curve increases as the axial force increases, against the dotted curve. It can be confirmed that the additional moment due to the vertical force should be taken into account in the moment of action.

https://doi.org/10.52202/069179-0416

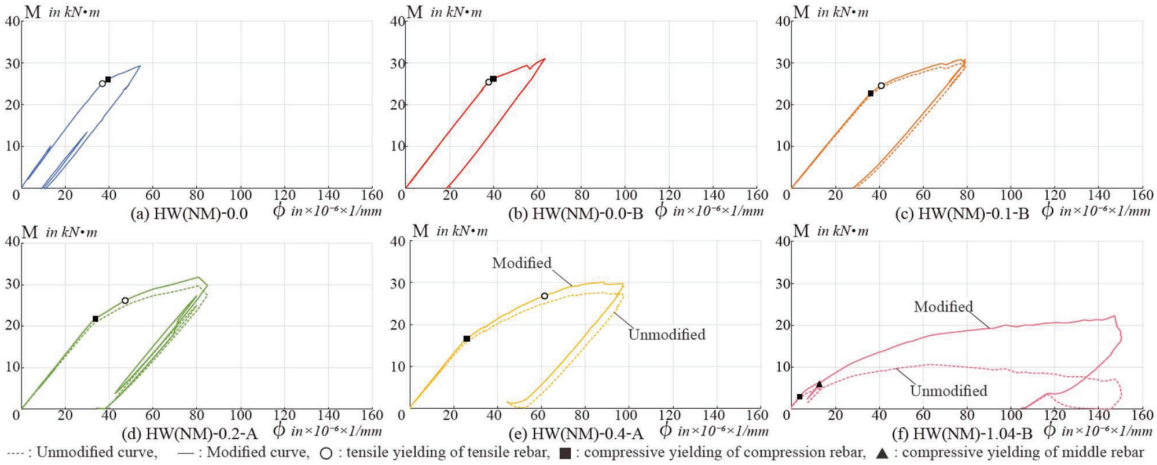

Figure 13: *Moment-curvature relationship*

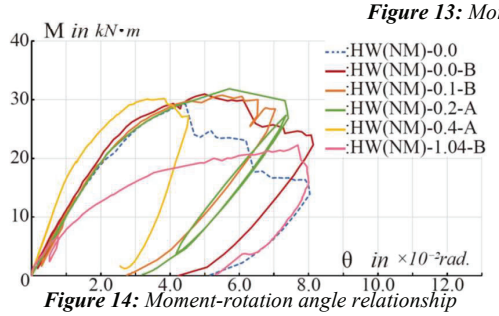

Figure 14: *Moment-rotation angle relationship*

Table 5: *Specimens, and experimental results of bending loading test for column*

Specimen	η	N	E	eMy	eMm
		in kN	*in N/mm²*	*in kN-m*	
HW(NM)-0.0	0.00	0.0	16041	25.0	29.3
HW(NM)-0.0-B	0.00	0.0	15903	25.4	30.9
HW(NM)-0.1-B	0.10	57.6	14990	22.7	30.7
HW(NM)-0.2-A	0.20	115.2	15202	21.8	31.9
HW(NM)-0.4-A	0.40	230.4	15087	16.6	30.1
HW(NM)-1.04-B	1.04	600.0	14775	3.0	22.3

η:Ratio of axial force, N:Axial force, E:Young's modulus, $_eM_y$:Yeilding moment, $_eM_m$:Bending capacity

Hereafter, the moments are described in terms of the additional moment.

The curvature was calculated from strain in the gauges on wood surface. The strain for curvature used average of the two strain gauges on a surface. The two values were in close agreement. The symbols '△',etc. indicate timings at which the strains at positions of tensile rebar, compression rebar, and middle rebar reached yielding strain of rebar, by using linear interpolation from values of the strain gauges on tensile and compressive surfaces.

The tensile rebar is indicated by symbol '○'; the compression rebar by symbol '□'; the middle rebar by symbol '△'. Tensile yield is indicated by white paint and compression yield by black paint. It was confirmed that when the axial force ratio was 0.00, yielding of tensile rebar or compressive rebar was almost simultaneous. However, as the axial force ratio increased, compressive yielding of the compression rebar preceded and yielding of the tensile rebar delayed. In the case of HW(NM)-1.04-B, of which the axial force was the highest of them, the tensile rebar did not yield and the middle rebar yielded in compression. Yielding of rebar is seen to decrease the stiffness. Bending moment at yielding decreased as the axial force increased, but the bending capacity tended to increase up to an axial force ratio of 0.2 and to decrease above that value. Table 5 lists experimental values of Young's modulus of column. The Young's modulus tended to decrease with increasing axial force. The maximum decrease is 8.9%, but it should be noted that yielding moment decreases significantly.

4.4.3 Moment-rotational angle relationship

Figure 14 shows moment-rotation angle relationship. HW(NM)-0.0, which was not reinforced with steel plates, is indicated by dotted line. HW(NM)-0.0 had the largest reduction of capacity after reaching maximum capacity because it accompanied rebar slip within the stub and wood split around rebar. HW(NM)-0.2-A and HW(NW)-0.4-A produced a less increase in rotation angle after the bending cracks. In HW(NM)-0.2-A and HW(NW)-0.4-A, the displacement transducer was fixed to the inner of the column section and deformation of bending cracks near the inner could not be included in the deformation, so the curves had less increase in the rotation angle after the bending crack. In the specimens reinforced with steel plate/B, two entrained displacement transducers (sensitivety:1 /10 mm) were installed to measure elongation and contraction between top stub and bottom stub, and the rotation angle was calculated from deformation by them.

5 BENDING TEST OF BEAM

5.1 AIM

Only material tests of the lamina were conducted in the column bending tests, and no bending tests of column of Glulam timber was conducted. Because bending strength of the Glulam timber could not be specified, experimental capacities of the column bending capacity could not be validated. Bending test by Glulam timber beams was conducted to capture relative relationship between strength of lamina and bending strength of Glulam timber in the column (cross section:150x150 mm).

5.2 CAUSE OF REDUCTION OF BENDING CAPACITY OF COLUMN SPECTIMN

As described in Section 4.4.1, failures were concentrated at the boundary between column and stub. The cause for this will be holes (diameter: 20mm) for the Glued-in-rod

to connect column to the stubs (hereinafter referred to as "insertion hole") drilled in column, and insertion holes close to the failure zone may have reduced bending capacity of Glulam timber.

5.3 SPECTIMN

Figure 15 shows shape and dimensions of beam specimen. Two types of specimens were employed: one Glulam timber beam and two Glulam beams with rebar inserted and glued at mid-span of the beam. The former was named as BWO and the latter as BWR-1 and BWR-2. The details of rebar and the insertion hole (diameter:20mm) were the same as those of the column specimen mentioned in Section 4.1. The lamina of the specimen also was the same species and grade, i.e., cedar/L50. However, the timing of fabrication of these specimens differed from that of the column specimens.

5.4 LOADING AND MEASUREMANT

Figure 16 illustrates set-up for loading and measurement. 4-point bending test was employed. Direction of bending was selected to be parallel to gluing layer of lamina as that of the column. Vertical deformation at the mid-span of beam, sinking deformations at left and right support points, and wood strain on upper and lower surfaces near the mid-span (length of inspection: 60 mm) were measured.

5.5 RESULTS

Figure 17 shows vertical force-deflection relationship at mid-span. The deflection was subtracted by deflection of both supports. The reduction in stiffness by inserted rebar is not clear, but maximum forces were reduced to 77.5% and 87.3% for BWR-1 and BWR-2 beams with rebar compared to that of Glulam timber beam (BWO). Figure 18 shows moment-curvature relationship of mid-span. The curvature was calculated from strain of foil strain gauges on upper and lower surfaces of timber. Figure 19 s hows positions of the foil strain gauges. Curvature in Figure 18(a) employed that of strain gauge away from the rebar/ (Location I). Bending stiffness of position away from the insert hole of rebar was hardly affected. The curvature in Figure 18(b) employed that of the location II close to the rebar. At the location, bending stiffness was reduced by the insert hole. Photo 4 shows final failures. Specimens with rebar had tensile cracks on at lower tensile surface as if connecting the insertion holes, whereas compressive portion by bending was never affected by the insertion holes because rebar and its adhesive produce compressive resistant. Figure 20 shows the relationship between moment and strain of foil strain gauges. Solid line indicates strain on lower tensile surface and dashed line dose strain of that on upper compression surface. In lower tensile surface, strain near the rebar was larger, while, in upper compression surface, strain was not affected by the rebar.

From these results, it can be concluded that, in compression zone by bending, bond interface between rebar and wood can resist compression, but, in tensile zone, the adhesive for rebar peels off at that of insertion hole and only wood's width excluding the sum of diameter of the hole can resist, resulting in a decrease in maximum bending capacity of Glulam timber beam.

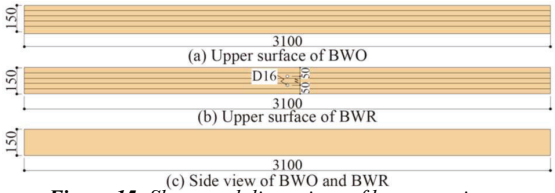

Figure 15: *Shape and dimensions of beam specimens*

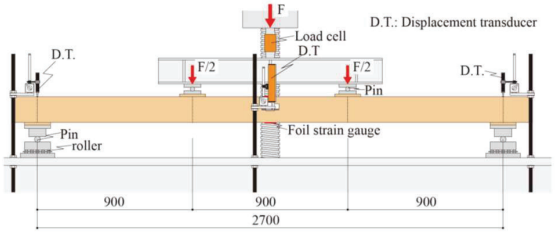

Figure 16: *Set-up for loading and measurement*

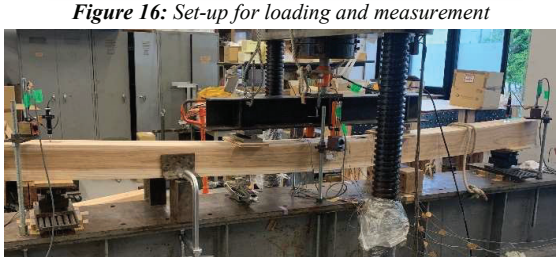

Photo 3: *Experiment situation*

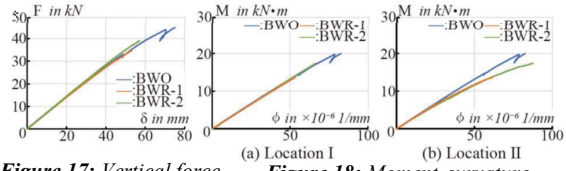

Figure 17: *Vertical force-deflection relationship of mid-span*

Figure 18: *Moment-curvature relationship*

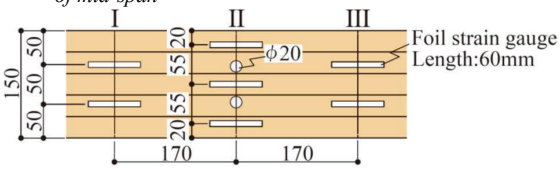

Figure 19: *Locations of the foil strain gauges*

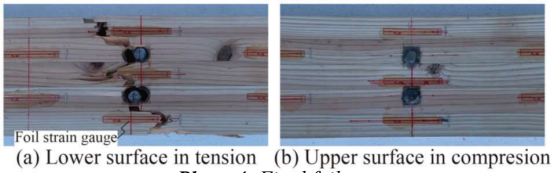

Photo 4: *Final failures*

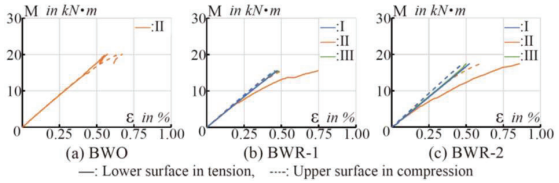

Figure 20: *The relationship between moment and strain of foil strain gauges*

5.6 BENDIG STRENTHS OF GLULAM TIMBER AND LAMINA

Figure 21in the next page shows resisting cross-section of beam for calculation of bending strength of timber at Location II. In BWR-1 and BWR-2, width equal to

https://doi.org/10.52202/069179-0416

diameter of the insertion hole was assumed to be unresisting over range from the neutral axis to lower tensile surface, and then the sectional modulus was calculated: the bending strength was calculated by dividing maximum moment using the modulus. Sectional modulus for BWO was calculated as a rectangular cross-section. The bending strength based on these calculations are indicated as horizontal lines in Figure 22. The bending strengths of BWO (solid line) and BWR-1 (dotted line) were almost the same, while that of BWR-2 (dashed line) was 1.11 times greater than BWO. The maximum force of BWR-1 was 0.78 times as much as that of BWO, and that of BWR-2 was 0.87 times as much as that of BWO. Therefore, it can be considered that bending strength of glulam timber can be identified more accurately by using the sectional modulus for effective cross-section in Figure 21. In the same figure, data of bending strength are plotted as symbol '△' and data of tensile strength are done as symbol '○' , by material tests of lamina. Figure 23 illustrates shapes and dimensions of the lamina testpiece. The numbers of bending and tensile specimens was 15 each. Tensile strength of BWO was 0.67 times as much as average of bending strengths and 1.20 times as much as average of tensile strengths.

It is well known that bending strength of glulam timber approaches tensile strength as its depth increases, and their magnification ratios correspond to this tendency. Figure 24 shows distribution of data of bending strength and tensile strength from material test of lamina testpieces of the column specimen described in Section 4.1.

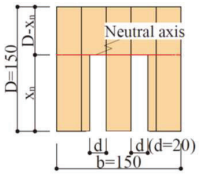

Figure 21: *Resisting cross-section area*

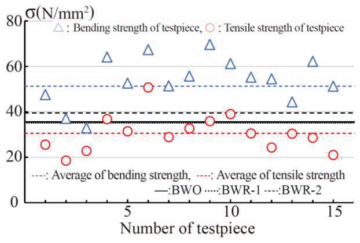

Figure 22: *Strength of lamina*

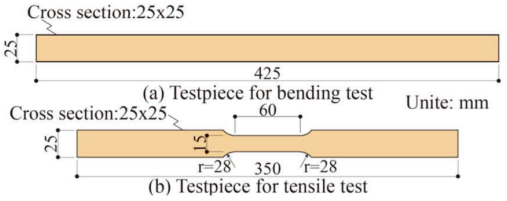

Figure 23: *Shapes and dimensions of the lamina testpiece*

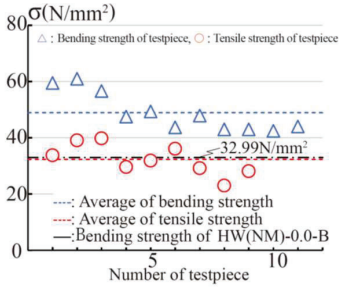

Figure 24 *Strength of column lamina by testpiece*

Similarly, comparing the mean values, tensile strength was 0.66 times as much as that of the bending strength. The bending strength of the Glulam timber calculated from HW-(NM)-0.0-B with zero axial force using the sectional modulus for Figure 21 is shown as a horizontal one dot chain line in Figure 24. In the calculation, Young's modulus of rebar was assumed to be the standard value of 2.05×10^5 N/mm^2, the yield strength of the rebar was done to be test value (384 N/mm^2), and Young's modulus of timber was done to be average/5530 N/mm^2 of Young's modulus by tensile and compression tests of lamina. Bending capacity was calculated using Equation (18) described later. In Figure 24, the horizontal one dot chain line is seen to be within range of data of tensile strength of lamina.

From above discussion, it can be concluded that it is reasonable to assume bending strength of Glulam timber to be 32.99 N/mm^2, which is the bending strength calculated from HW(NM)-0.0-B by Young's modulus of average of experimental values of the tensile testpieces and the sectional modulus for Figure 21.

6 AXIAL FORCE-BENDING CAPACITY CORRELATION CURVE

6.1 EXPERIMENTAL RESULTS

Figure 25 plots data of axial force and yielding moment with symbol '○' and data of axial force and bending capacity with symbol '●'. The experimental values for compression test of column were plotted with bending capacity being zero. Yielding moment employed bending moment at which rebar yielded on the moment-curvature relationship in Figure 13. Bending capacity employed maximum bending moment. HW(NM)-0.0 without steel plate reinforcement is indicated by symbols '△' or '▲'. The yield moment decreases linearly with increasing axial force. On the other hand, the bending capacity increases over range of axial force ratio/ η of 0.0-0.2, but rather increases and decreases when η is 0.4 or higher.

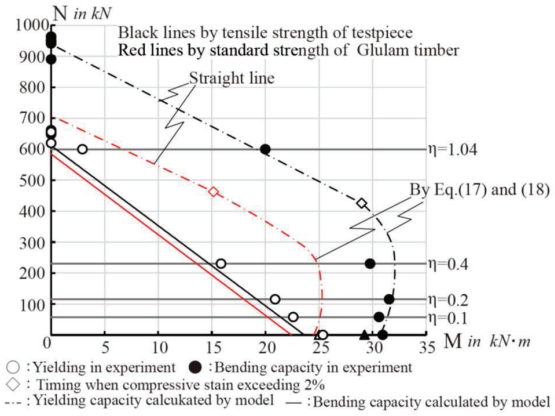

Figure 25: *Axial forth-bending capacity correlation curve*

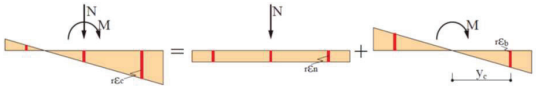

Figure 26: *Model of bending strain distribution*

https://doi.org/10.52202/069179-0416

6.2 ESTIMIATION FOR YIELD MOMENT

Figure 26 illustrates a model of bending strain distribution in a column section. Except when axial force is zero, compression rebar yields first because axial force/N and bending moment/M act simultaneously. The moment can be estimated as moment at which compression rebar yields. Even if axial force is zero, yielding moment can be estimated on the assumption that tensile yielding of tensile rebar and compressive yielding of compression rebar occur simultaneously in a symmetrical cross-section. Strain ${}_r\varepsilon_c$ of compression rebar is the sum of the strain ${}_r\varepsilon_n$ by axial force and the strain ${}_r\varepsilon_b$ by bending moment. ${}_r\varepsilon_n$ and ${}_r\varepsilon_b$ are expressed by Equations (2) and (3) .

$$ {}_r\varepsilon_c = {}_r\varepsilon_n + {}_r\varepsilon_b \quad (1) $$

$$ {}_r\varepsilon_n = N/A_e \cdot 1/E_w \quad (2) $$

$$ A_e = b \cdot D + (n-1) \cdot \Sigma a_r $$

$$ {}_r\varepsilon_b = \phi \cdot y_c $$

$$ = M/(E_w \cdot Ie) \cdot y_c \quad (3) $$

where, b: column width, D: column depth, n: Young's modulus ratio (=E_r/E_w), E_r: Young's modulus of rebar, E_w: Young's modulus of timber, a_r: area per rebar, ϕ : curvature, y_c: distance from neutral axis to compression rebar, I_e: sectional secondary moment of column including effect of rebar.

Strain ${}_r\varepsilon_y$ of rebar which reaches the yield stress/σ_y can be expressed by dividing σ_y by the Young's modulus/E_r of the rebar by using Equation (4).

$$ {}_r\varepsilon_y = \sigma_y/E_r \quad (4) $$

Substituting this ${}_r\varepsilon_y$ into ${}_r\varepsilon_c$ in Equation (1), yield moment/M_y in which stress in the rebar reaches yielding stress/σ_y is finally expressed as Equation (5).

$$ M_y = (\sigma_y/n - N/A_e) \cdot I_e/y_c \quad (5) $$

6.3 ESTIMATION FOR BENDING CAPACITY

6.3.1 Rapture strain of wood in bending capacity

Figure 27 shows bending moment-strain relationship of the column specimen. Moments were assumed to be moments taking axial force into account. The strain was taken as foil strain gauge value.

For HW(NW)-0.0 and HW(NW)-0.0-B with zero axial force, the magnitude of compressive strains on compression surface and tensile strains in tensile surface at the maximum bending moment were almost identical: the former was -0.40% and the latter was 0.55%.

For HW(NM)-1.04-B, where the axial force was the greatest of them and its wood did never fail in tension by bending, the strain at the compression surface increased up to -1.80 to -1.95%, but the strain at the tensile surface was only 0.42%. The maximum strain at the tensile of HW(NM)-0.0, where the rebar slip-failed at the stub without steel plates, was still only 0.42%.

From these results, it can be concluded that if bending capacity is determined by tensile rupture by bending, the tensile strain of wood of the tensile surface by bending can be assumed to be 0.5%.

6.3.2 Stress-strain relationship of wood

Figure 28 shows stress-strain curves for compression and tensile tests for testpiece of lamina of the column specimen. In only one testpiece of compression test, compressive strength was maintained up to approximately 2% of strain after compressive yielding. However, as seen in Figure 6, rebar boosts the strain up to approximately 2%. Roughly, the relationship can be assumed to be fully elastoplastic. In tensile test, wood ruptures immediately when the tensile strength is reached.

On the basis of these results, stress-strain relationship of wood in compression and tension, adopted as a model for estimation of bending capacity, are shown in Figure 29(a).

6.3.3 Equation for estimation of bending capacity

Figure 29(b) illustrates an assumed stress distribution of column at bending capacity. Timing when strain of tensile surface by bending reaches 0.5% is assumed to be timing of bending capacity. The distance/x_n from the compression surface to neutral axis is expressed in Equation (6).

$$ x_n = -\varepsilon_c/(\varepsilon_t - \varepsilon_c) \cdot D \quad (6) $$

where ε_c: strain on compression surface by bending, ε_t: strain on tensile surface, D: column depth

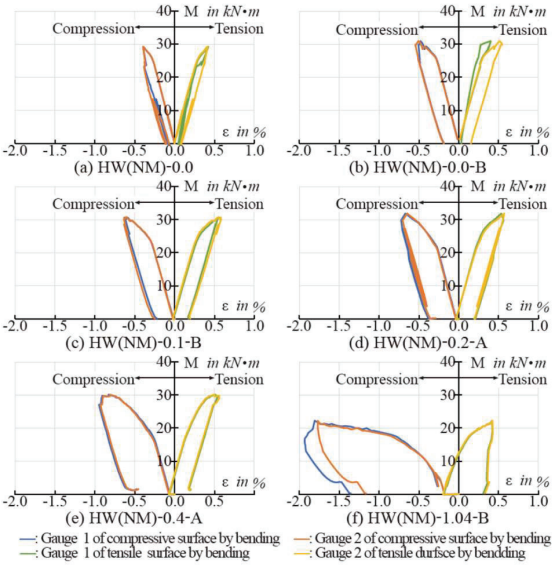

Figure 27: *Bending moment-strain relationship*

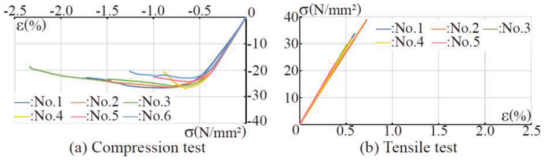

Figure 28: *Stress-strain relationships of lamina*

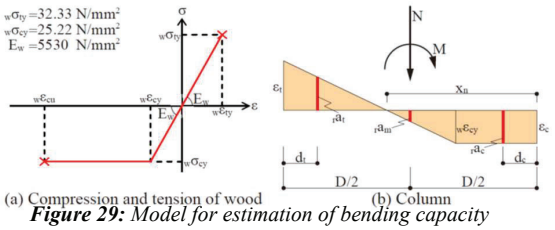

Figure 29: *Model for estimation of bending capacity*

https://doi.org/10.52202/069179-0416

Strain/$_r\varepsilon_c$ of rebar on the compression, strain/$_r\varepsilon_t$ of rebar on the tension, and strain $_r\varepsilon_m$ of middle rebar at column depth are expressed by Equations (7)-(9), respectively.

$$_r\varepsilon_c=\varepsilon_c\cdot(x_n-d_c)/x_n \quad (7)$$

$$_r\varepsilon_t=\varepsilon_t\cdot(D-x_n-d_t)/(D-x_n) \quad (8)$$

$$_r\varepsilon_m=\varepsilon_c\cdot(x_n-0.5\cdot D)/x_n \quad (9)$$

where d_c: distance from compression surface to its near rebar, d_t: distance from tensile surface to its near rebar.

Resultant force/$_rT$ of rebars in tension, resultant force/$_rC$ of rebars in compression, and resultant forcer/$_rC_m$ of rebars in the middle at column depth are expressed by equations (10)-(12), respectively.

$$_rT=E_r\cdot{}_r\varepsilon_t\cdot{}_ra_t \quad (10)$$

$$_rC=E_r\cdot{}_r\varepsilon_c\cdot{}_ra_c \quad (11)$$

$$_rC_m=E_r\cdot{}_r\varepsilon_m\cdot{}_ra_m \quad (12)$$

where $_ra_t$: cross-sectional area of tensile rebar
$_ra_c$: cross-sectional area of compression rebar
$_ra_m$: cross-sectional area of middle rebar

Resultant force/$_wT$ of wood in tension and resultant force/$_wC$ of wood in compression are expressed by Equations (13) and (14).
The compression range can be divided into a constant section and the other section like a triangle because there is a section where stress level is constant within assumed stress-strain relationship of wood.

$$_wT=0.5\cdot{}_w\sigma_{ty}\cdot b\cdot(D-x_n) \quad (13)$$

$$_wC={}_wC_1+{}_wC_2 \quad (14)$$

$$_wC_1=0.5\cdot{}_w\sigma_{cy}\cdot b\cdot{}_w\varepsilon_{cy}/\varepsilon_c\cdot x_n \quad (15)$$

$$_wC_2={}_w\sigma_{cy}\cdot b\cdot(\varepsilon_c-{}_w\varepsilon_{cy})/\varepsilon_c\cdot x_n \quad (16)$$

where $_w\sigma_{ty}$: tensile strength of wood, $_w\sigma_{cy}$: compressive strength of wood, $_w\varepsilon_{cy}$: strain of wood at its compressive strength

Axial force balance is given by Equation (17), and bending capacity/M_u is given by Equation (18).

$$N+{}_rT+{}_wT={}_rC_m+{}_rC+{}_wC \quad (17)$$

$$\begin{aligned}Mu=&{}_rT\cdot(0.5\cdot D-d_t)+{}_wT\cdot(0.5\cdot D-1/3\cdot(D-x_n))\\&+{}_rC\cdot(0.5\cdot D-d_c)+{}_wC_1\cdot(0.5\cdot D-(1/3\cdot x_n\\&\cdot{}_w\varepsilon_{cy}/\varepsilon_c+x_n\cdot(\varepsilon_c-{}_w\varepsilon_{cy})/\varepsilon_c))\\&+{}_wC_2\cdot(0.5\cdot D-0.5\cdot x_n\cdot(\varepsilon_c-{}_w\varepsilon_{cy})/\varepsilon_c)\end{aligned} \quad (18)$$

6.4 COMPARISON OF CALCULATION AND EXPERIMENTAL VALUES

In Figure 25, correlation curves of axial force-yield moment by solid line and axial force-bending capacity by single-dotted curve are shown. The black curves were calculated on the basis of strength and resisting cross-section mentioned in Section 5.6. However, as the axial force increases, the strain of the compression surface exceeds the limit of strain (2.0%). For higher axial forces, the curve was assumed to be approximated by a straight line connecting the point and the point of uniaxial compression capacity with bending being zero. Yield moment tends to decrease linearly as axial force increases, and bending capacity curve has a maximum value at an axial force ratio/ η of approximately 0.3, which is consistent with experimental trend. Calculated curves are generally in agreement with experimental values. Red curves using standard values for rebar (SD345) and cedar laminated wood (E65-F225) are evaluated on the safe side. For wood, compressive strength on compressive zone was assumed as compressive strength, whereas tensile strength on tensile zone was assumed as bending strength.

7 SUMMARY

In order to develop estimation method of yield moment and bending capacity for the steel bar-timber composite column subjected to axial compression and bending moment for column of story above second story in building, compression test and bend test of column, and bend loading test of Glulam timber beam were conducted by specimens scaled as 25%. The results are summarized as followings:

i) Compression capacity and stiffness of column increase as the amount of rebar increases. Also, ductility of compression increases slightly and become stable.
ii) Yield bending moment decreases linearly as axial force increases whereas bending capacity varies as a curve with a peak at axil force ratio being approximately 0.3.
iii) Bending capacity of column was estimated more accurately when duct of wood in column due to joint rebar for connection stub to column was taken account. This suggests that column-beam connection in building should also take account for the duct by bolts or glued-in rod used in the connection.
iv) Formula for estimation of bending yield moment and bending capacity of column with increasing axial force were proposed, and the correlation curve by using the formulas and tensile properties of lamina estimated accurately experimental data. By using standard values of Glulam timber, the curve estimated the experimental data on the safe side.
v) The ratios of tensile strength, compressive strength of lamina, and bending strength of glulam timber were identified. Tensile strength of timber by bending of glulam timber can be estimated to be close to the tensile strength of lamina and the compressive strength of the wood in the compression zone by bending can be done to be close to the compressive strength of lamina.

ACKNOWLEDGEMENT

This project was funded as Grants-in-Aid for Scientific Research ‘A’ by Japan Society for the Promotion of Science, 2022.

REFERENCE

[1] S.Shioya, et al. : An innovative hybrid timber structure in Japan: performance of column and beam, WCTE 2016.
[2] M. Mukai, et al. : Horizontal-loading test of steel bar-timber composite column for mid-rise building, WCTE 2021.
[3] K. Mori, S. Shioya: Stiffness and strength of full-scale steel bar-timber composite beams with comparative small-depth, WCTE 2021.
[4] N. Fukutomi, S. Shioya: Design method to estimate stiffness and strength of hybrid timber-steel bar beams, WCTE 2018.